High-sensitivity Rydberg atom-based phase modulation receiver for frequency division multiplexing communication

Yafen Cai,[1, a)] Shuai Shi,[1, a)] Yijia Zhou,[1, a)] Yitong Li,[1, a)] Jianhao Yu,[1] Weibin Li,[1] and Lin Li[1]

(*Electronic mail: li_lin@hust.edu.cn)

(*Electronic mail: weibin.li@nottingham.ac.uk)

(Dated: 15 March 2023)

Due to the exaggerated properties of highly excited atomic states, Rydberg atom-based microwave receiver holds the promise to achieve superior performances in microwave metrology and communication when compared to conventional antennas. However, developing long-distance communication applications based on Rydberg atomic receiver remains challenging, because it requires the simultaneous achievement of low bit error rate (BER), high symbol rate, and weak carrier amplitude. The key to tackle this problem is to encode the information with a proper scheme that maintains high sensitivity and robustness of the Rydberg atomic receiver. Here, we use Rydberg atom-based heterodyne detection for the reception of phase-modulated microwave field, and demonstrate more than one order of magnitude improvement in reception sensitivity compared to the previously investigated amplitude modulation scheme. Therefore, we achieve low BER communication with high symbol rate of 12 kSym/s and weak carrier amplitude of 13 μVcm^{-1} simultaneously. Furthermore, we also demonstrate that our scheme is compatible with frequency division multiplexing communication.

I. INTRODUCTION

Rydberg atom has wide applications in microwave (MW) electrometry for weak-field sensing and wireless communication. The characteristic feature of Rydberg atoms is their rich orbital states with large principal quantum numbers. The transition frequencies between those Rydberg states cover wide MW spectral spanning from MHz to 1 THz[1,2]. Due to the large orbital radii, the polarizability of the Rydberg states is also significantly larger than the ground states, which leads to high sensitivity of 12.5 nVcm^{-1}Hz$^{-1/2}$[3]. Moreover, the detection of the MW field does not rely on the absorption of the MW field itself, but on the energy shift of the Rydberg states via the electromagnetically induced transparency (EIT)[4]. This non-destructive process allows the Rydberg sensors to exceed the Chu limit in the conventional dipole antenna[5], and is important to avoid the electromagnetic interference and miniaturize the whole device. Recently, many electric-field sensing schemes with Rydberg atoms have been proposed and demonstrated involving periodic modulation[5–10], which show their advantages over traditional dipole antennas including high sensitivity, broad operating frequency range and non-destructive interactions with the MW field[11].

Previously, amplitude modulation (AM)[11–13] and frequency modulation (FM)[9,14] based schemes are used for enconding information in the MW fields. For AM scheme, the photon-shot-noise limited Rydberg receiver has achieved the symbol rate 10 kSym/s with the carrier field amplitude being 130 μVcm^{-1}[13]. For FM scheme, the optical readout from the Rydberg atomic receiver with a 1 kHz sinusoidal baseband signal FM-modulated onto the carrier at 63 mV/cm is demonstrated[14]. In conclusion, the AM and FM schemes are based on the response of the Rydberg atomic spectrum to carrier amplitude and frequency. So the AM and FM communication schemes are vulnerable to undesirable disturbance in carrier amplitude. While the fluctuation of carrier amplitude in long-distance communications is inevitable and then results in wrong decoding.

To avoid the effect of carrier amplitude noise on communication performance, PM scheme can been employed in Rydberg atomic receivers. In addition, heterodyne detection technique is utilized to improve the reception sensitivity. Therefore, the Rydberg receiver with PM scheme can achieve greater communication range that not only reduces the number of communication base stations but also improves wireless communication security. Here, we theoretically and experimentally investigate the phase modulation (PM) scheme, which can simultaneously achieve high channel capacity under weak carrier field. What's more, frequency division multiplexing is demonstrated to improve the channel capacity of the Rydberg atomic receiver.

We experimentally implement the high-sensitivity MW receiver based on ^{87}Rb Rydberg atoms using the PM scheme, and further compare with the phase-sensitive AM scheme[13]. First, we show that the response of the beat signal from Rydberg atomic receiver to carrier amplitude is linear in the PM scheme, but near quadratic in the AM scheme, which can be proven theoretically and accounts for the better performance of the PM scheme. Then, the practical performance is demonstrated by transmitting a digital image and measuring the error pixels to obtain the BER. The result shows that the minimum carrier amplitude that ensures clear communication for the PM scheme is more than one order of magnitude smaller than that of AM scheme. In other words, the communication range of the PM scheme can be improved by more than one order of magnitude. For the PM scheme, the BER is less than 5% for minimum carrier amplitude of 13 μVcm^{-1} and symbol rate of 12 kSym/s. Finally, we improve the channel capacity by implementing frequency division multiplexing and an 8-state phase-shift-keying digital modulation scheme.

[a)]These authors contributed equally.

II. COMMUNICATION PROTOCOL BASED ON RYDBERG RECEIVER

The three extensively used modulation schemes for digital communication are amplitude shift keying (ASK), frequency shift keying (FSK), and phase shift keying (PSK). In recent years, significant progress has been made in Rydberg atomic receiver[5–10,12,13]. Particularly, ASK schemes are widely investigated in previous works, where the digital information is encoded in the amplitude of the carrier. During the decoding process, the Rydberg atomic receiver measures the carrier amplitude to recover the digital information. The reliability of ASK scheme lies in the carrier amplitude stability, which is vulnerable to environmental disturbance. For the FSK scheme, the digital information is encoded in the carrier frequency. The Rydberg atomic receiver can decode the information by converting the carrier frequency to the transmission of the probe laser. While the probe laser transmission depends on carrier amplitude too. Therefore the FM communication scheme is also very sensitive to carrier amplitude. Two forms of PSK schemes can be used to solve this problem. One is encoding the information in the phase of the AM and receiving it via nonlinear detection[13]. The other is directly encoding the information in the phase of carrier and receiving it via heterodyne detection. In this work, we experimentally implement these two forms PSK schemes and compare their reception sensitivity quantitatively.

The PSK scheme based on nonlinear detection is performed by switching the weak carrier at a frequency of δf, and the digital information is encoded in the phase of the MW switch signal. Once the modulated MW interacts with Rydberg atoms, the atomic transmission spectrum changes correspondingly. Due to the nonlinear response of probe laser transmission to carrier amplitude when the Rabi frequency of carrier is smaller than the linewidth of the EIT spectrum, the standard atomic electrometer for weak MW fields is nonlinear and termed as nonlinear detection[13,15]. The phase of the MW switch can be extracted from the atomic transmission spectrum with the aid of a lock-in amplifier.

The PSK scheme based on heterodyne detection is performed by introducing a strong local (LO) MW field, and the digital information is encoded in the phase of the carrier directly. The carrier is detuned from the LO MW field with a frequency of δf. Then the carrier is measured by Rydberg atom-based heterodyne detection. The phase of the heterodyne signal corresponds to the relative phase between the LO and carrier. Therefore, the digital information encoded in the phase of the carrier can be extracted from the atomic spectroscopy in real-time with the aid of a lock-in amplifier.

III. EXPERIMENTAL SETUP AND RESULTS

The schematic of the experiment is shown in Fig. 1. The counter-propagating probe (780 nm) and control (480 nm) lasers are employed to form a ladder-type EIT in a ^{87}Rb vapor cell. The opposite directions of the two lasers can minimize the Doppler broadening. The probe and control lasers

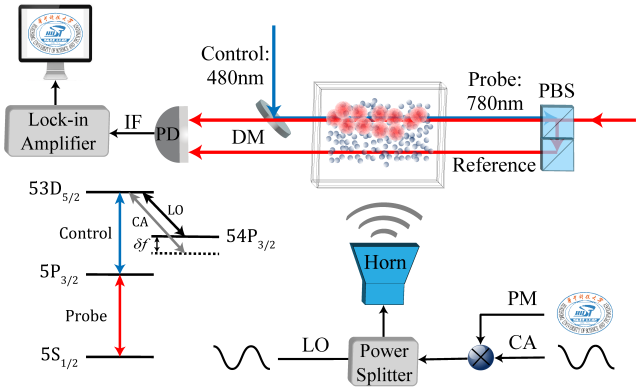

FIG. 1. Schematic of the PM Rydberg atomic receiver. The counter-propagating probe and control lasers form a ladder-type EIT spectrum in a vapor cell. A reference 780 nm laser is employed to suppress the high-frequency intensity noise of the probe laser. The strong LO MW and phase-modulated carrier were combined by a MW power splitter. MW fields emitted from the horn antenna couple the $|r_1\rangle = |53D_{5/2}\rangle$ and $|r_2\rangle = |54P_{3/2}\rangle$ Rydberg states. The relative phase between the LO MW field and carrier is recorded by a balanced photodetector and measured by a lock-in amplifier. The inset shows the energy levels of ^{87}Rb involved in the experiment. The LO MW field is resonant with the Rydberg transition. While the carrier is detuned from Rydberg transition by δf. Abbreviations: DM: dichroic mirror; PD: photodetector; LO: local field; CA: carrier; PM: phase modulation.

resonantly couple $|g\rangle \leftrightarrow |e\rangle$ ($|5S_{1/2}, F = 2\rangle \leftrightarrow |5P_{3/2}, F = 3\rangle$) and $|e\rangle \leftrightarrow |r_1\rangle$ ($|5P_{3/2}, F = 3\rangle \leftrightarrow |53D_{5/2}\rangle$) transitions, respectively. The probe transmission is detected by a balanced photodiode with the aid of a reference beam, which can suppress the high-frequency intensity noise of the probe laser and eliminate the DC offset of the atomic transmission spectrum. The MW fields at 14.234 GHz emitted from the horn drive the Rydberg transition between $|r_1\rangle = |53D_{5/2}\rangle$ and $|r_2\rangle = |54P_{3/2}\rangle$. In addition, the polarization of both lasers and MW fields are linear and parallel to each other.

Rydberg atom-based heterodyne detection enables accurate phase measurement of MW field and paves the way for PM communication scheme. Heterodyne detection is performed by interfering the carrier with a strong LO MW field. The LO MW field is resonant with the Rydberg transition and induces two MW-dressed Rydberg states $|\pm\rangle = (|r_1\rangle \pm |r_2\rangle)/\sqrt{2}$. The energy gap between the dressed states is proportional to the LO MW field amplitude. The presence of the detuned carrier modulates the total MW field amplitude that interacts with the Rydberg atoms, and leads to the energy gap of the MW-dressed states oscillating at the detuning frequency δf. The modulation of the total MW field amplitude is mapped to the atomic transmission spectrum. Then, the Rydberg atoms act as a MW mixer[16] and down-convert the input LO and carrier. The interference signal at frequency δf in the atomic transmission spectrum is termed as intermediate frequency (IF) signal. To maximize IF signal, the amplitude of the LO MW field is optimized experimentally. According to previous work[15], the energy gap between the MW-dressed states caused by the optimal LO MW field amplitude approaches

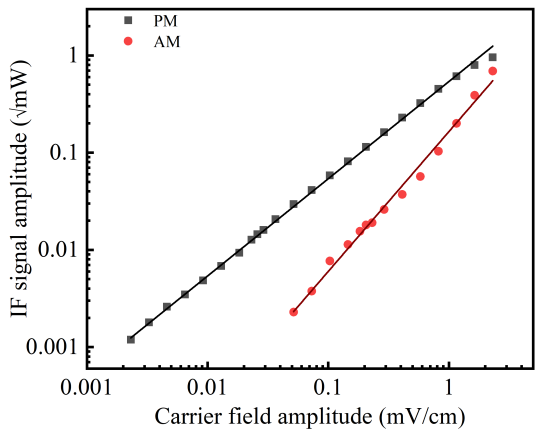

FIG. 2. Phase modulation scheme versus amplitude modulation scheme. A strong LO MW is introduced for the phase modulation scheme to achieve heterodyne detection. The beat signal amplitude as a function of carrier amplitude is recorded as gray squares, and the solid gray line is a linear fit with a slope of 1. For comparison, we converted our experiment set-up to AM communication scheme. A switch modulates the MW amplitude and thereby changes the atomic spectrum[13]. The corresponding intermediate frequency signal amplitude as a function of carrier amplitude is shown as red circles. The red line shows a nearly quadratic fitting.

the EIT linewidth.

As shown in Fig. 2, the sensitivity is compared between nonlinear detection and heterodyne detection by measuring the amplitude of IF signal with different carrier amplitude. In this work, we set $\delta f = 100\,\mathrm{kHz}$, and measure the amplitude of IF signal via a spectrum analyzer with 1 Hz resolution bandwidth. The experimental results of the IF signal amplitude under different carrier amplitude are shown by the gray squares in Fig. 2. The amplitude of IF signal linearly increases with the carrier amplitude, and the solid gray line indicates a linear fit with a fixed slope of 1. By contrast, the nearly quadratic scaling of the IF signal amplitude with carrier amplitude in nonlinear detection protocol is predicted in Ref[15]. As shown by the red circles in Fig. 2, we measured and verified the nearly quadratic scaling of IF signal amplitude with carrier amplitude in AM scheme. As a result, the PM scheme generates a stronger signal than the AM scheme and is significantly more sensitive to the weak carrier field due to its linear response.

In the weak excitation regime, the power law scaling of the IF signal versus carrier amplitude can be derived from Floquet theory. The Floquet space is spanned from the original four-level system which consists of $|i,m\rangle$ where $i = g,e,r_1,r_2$ encodes the atomic internal state and $m = 0,\pm1,\pm2,\cdots$ represents for the oscillation frequency. The first order response that picked up by the heterodyne detection is dominated by the transitions of $|g,0\rangle \to |e,0\rangle \to |r_1,0\rangle \to |r_2,0\rangle \to |r_1,\pm1\rangle \to |e,\pm1\rangle$ and $|g,0\rangle \to |e,0\rangle \to |r_1,0\rangle \to |r_2,\pm1\rangle \to |r_1,\pm1\rangle \to |e,\pm1\rangle$. For PM scheme, the coupling strengths of the five transition steps are $\Omega_p, \Omega_c, \Omega_{\mathrm{LO}}(\Omega_{\mathrm{sig}}), \Omega_{\mathrm{sig}}(\Omega_{\mathrm{LO}}), \Omega_c$, respectively. Therefore, the signal of the PM scheme is proportional to $\sim \Omega_p\Omega_c^2\Omega_{\mathrm{LO}}\Omega_{\mathrm{sig}}$. For AM scheme, however, with the absence of the LO MW field, the coupling strengths are $\Omega_p, \Omega_c, \Omega_{\mathrm{sig}}/2, \Omega_{\mathrm{sig}}/2, \Omega_c$, respectively. Therefore, the signal of the AM scheme is proportional to $\sim \Omega_p\Omega_c^2\Omega_{\mathrm{sig}}^2$ (see **SM** for details).

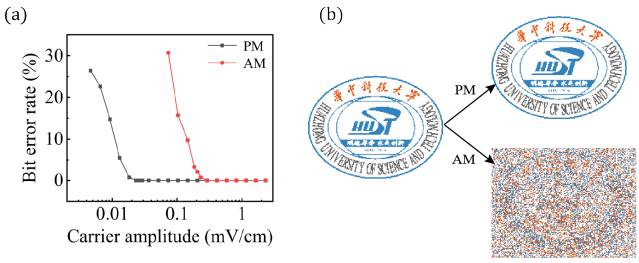

FIG. 3. (a) Bit error rate for image data reception at different carrier amplitude. The gray squares and red circles indicate the result of PM and AM communication schemes, respectively. The minimum carrier amplitude to ensure reliable transmission of digital information for the PM scheme is more than one order of magnitude lower than the AM communication protocol. (b) The left part is the original transmitted image, which is the logo of Huazhong University of Science and Technology and 200×150 pixels Portable Network Graphics (PNG) with lossless compression. The right top one shows that the bit error rate of the recovered image of the PM scheme is 0. While the right bottom one demonstrates that the retrieved logo image is distorted severely by employing the AM transmission scheme. The carrier amplitudes of the AM and PM schemes used for image transmission are identical for comparison.

IV. PERFORMANCE OF THE HIGH-SENSITIVITY RYDBERG ATOMIC RECEIVER

In order to compare the reception sensitivity of the AM scheme and PM scheme, we transmit an image data and compare the quality of the received image by BER. BER is defined as the number of error bits divided by the total transmitted bits Bit error usually results from distortion and attenuation of the carrier during transmission[17]. Therefore, the BER becomes higher as the increase of transmission distance. Communication range is one of the most important parameters for wireless communication and depends on the reception sensitivity of receiver.

We fix the symbol rate to be 12 kSym/s for both AM and PM schemes, and evaluate the communication performance by the BER under different carrier field amplitude for image reception. As shown in Fig. 3, the BER gets higher when decrease the carrier amplitude for both AM and PM schemes. The reception sensitivity is defined as the minimum carrier amplitude that guarantees the BER less than 5%[9]. As shown by the gray squares in Fig. 3(a), the reception sensitivity of PM scheme is $13\,\mu\mathrm{V/cm}$, which is more than one order of magnitude better than that of AM scheme. In conclusion, our PM communication scheme is superior for weak field communication and paves the way for practical application of Ry-

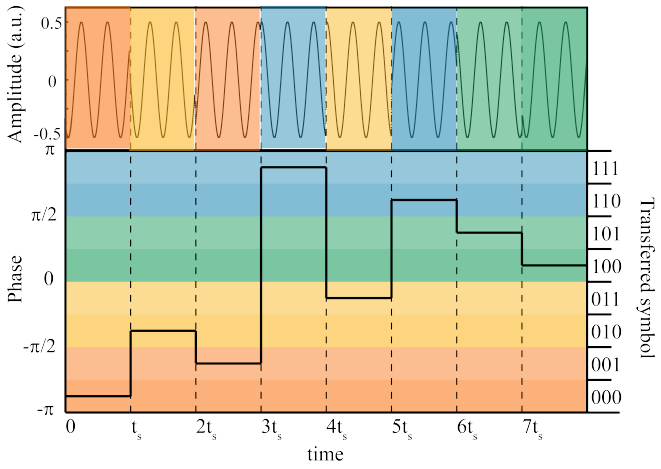

FIG. 4. The transferred 3-bit digital symbol is encoded in the phase of the carrier. In the experiment, the carrier phase is received by Rydberg atomic sensor and extracted from the probe transmission spectrum with the aid of a lock-in amplifier. Finally, the transmitted symbol is decoded by mapping the extracted MW phase to digital information according to the right axis. The phase range covered by a digital symbol is $\pi/4$.

dberg atomic receiver.

To visually demonstrate the PM scheme's advantage in practical communication performance, the image of a logo is transmitted by AM and PM schemes with the same carrier amplitude, respectively. As shown in Fig. 3b, the transferred information is 200×150 pixels in size. For a carrier at $23\,\mu V/cm$, the decoded results are shown in Fig. 3b for PM and AM communication schemes, respectively. The recovered image from AM communication scheme is distorted severely. On the contrary, the decoded image from PM scheme is clear and free from any visible error.

Besides reception sensitivity, another important parameter for a communication receiver is the maximum channel capacity. Rydberg atom-based MW receiver can support 8-PSK with low BER. As shown in Fig. 4, 8-PSK uses eight different phase states to transmit data. The correspondence between carrier phase and digital data is $-157.5°$ (state "000"), $-112.5°$ (state "001"),$-67.5°$ (state "010"),$-22.5°$ (state "011"),22.5° (state "100"),67.5° (state "101"),112.5° (state "110"),157.5° (state "111").

Furthermore, we demonstrate that the channel capacity can be improved by using the frequency division multiplexing technology. By utilizing carriers with different frequencies to transmit data simultaneously and independently, we experimentally demonstrate that the data capacity of the frequency division multiplexing system increases with the channel numbers. We let three carriers combined by a power combiner and coupled to free space via a horn antenna. As shown in Fig. 5, three carriers transmit different digital information simultaneously and independently. As shown in Fig. 5b-d, the detected digital information in various carriers is distinguished from each other by IF signal frequency. In order to avoid the disturbance between different carriers, the symbol rate should be lower than half of the smallest frequency gap between carriers. Otherwise, the BER will increase dramatically.

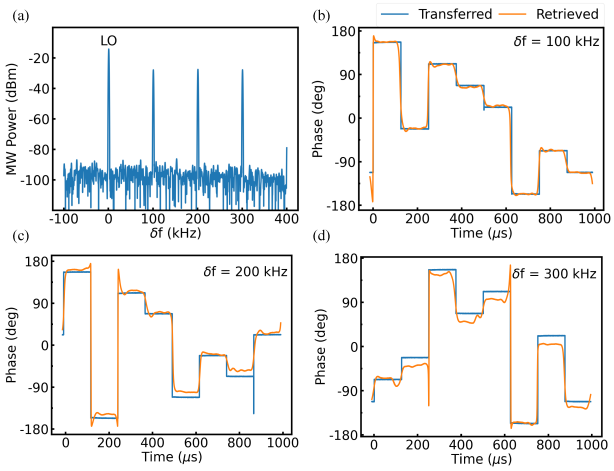

FIG. 5. The three channels frequency division multiplexing is achieved in one compact set-up with Rydberg atomic sensor. Plots (a)-(c) show different digital information transmitted by the three carriers simultaneously and independently. The solid blue line shows the transmitted digital information. The red line indicates the retrieved data. (d) shows the spectrum of the LO MW field and three carrier that detected by the spectrum analyzer.

V. CONCLUSION

We have demonstrated a high-sensitivity PM communication scheme and empirically measured the minimum carrier amplitude for reliable communication. The results show that the PM is superior to the AM scheme in reception sensitivity. The carrier amplitude that ensures reliable communication for our PM scheme is more than one order of magnitude smaller than that of AM schemes. The physical reason for the improvement results from the fact that the PM scheme has linear response to the modulated MW field while the AM scheme responds quadratically. Furthermore, we have realized the frequency division multiplexing Rydberg atomic receiver in a compact vapor cell and analyzed the crosstalk between adjacent MW carriers qualitatively.

The PM Rydberg atomic sensor features a large communication range and is electromagnetic-interference-free, which extends the practical application of the quantum receiver, such as reducing the number of the wireless base station for 5G communication. Moreover, implementing the frequency division multiplexing technique could vastly improve the reception data rate.

ACKNOWLEDGMENTS

This work is supported by the National Key Research and Development Program of China under Grants No. 2021YFA1402003 and the National Natural Science Foundation of China (Grant No. U21A6006, No. 12004127,

No. 12004126, No. 12005067 and No. 12104173). W. L. acknowledges support from the EPSRC through Grant No. EP/R04340X/1 via the QuantERA project "ERyQSenS" the UKIERI-UGC Thematic Partnership (IND/CONT/G/16-17/73), and the Royal Society through the International Exchanges Cost Share award No. IEC\NSFC\181078. Y. Z. is supported by National Natural Science Foundation of China (Grant No. 12088101), and NSAF (Grant No. U1930403)..

DATA AVAILABILITY STATEMENT

The data that support the findings of this study are available from the corresponding author upon reasonable request.

AVAILABILITY OF DATA	STATEMENT OF DATA AVAILABILITY
Data available on request from the authors	The data that support the findings of this study are available from the corresponding author upon reasonable request.

[1] Y.-Y. Jau and T. Carter, "Vapor-cell-based atomic electrometry for detection frequencies below 1 khz," Phys. Rev. Applied **13**, 054034 (2020).
[2] D. H. Meyer, Z. A. Castillo, K. C. Cox, and P. D. Kunz, "Assessment of rydberg atoms for wideband electric field sensing," Journal of Physics B: Atomic, Molecular and Optical Physics **53**, 034001 (2020).
[3] M. Cai, Z. Xu, S. You, and H. Liu, "Sensitivity improvement and determination of rydberg atom-based microwave sensor," Photonics **9** (2022), 10.3390/photonics9040250.
[4] J. A. Sedlacek, A. Schwettmann, H. Kübler, R. Löw, T. Pfau, and J. P. Shaffer, "Microwave electrometry with rydberg atoms in a vapour cell using bright atomic resonances," Nat. Phys. **8**, 819–824 (2012).
[5] K. C. Cox, D. H. Meyer, F. K. Fatemi, and P. D. Kunz, "Quantum-limited atomic receiver in the electrically small regime," Phys. Rev. Lett. **121**, 110502 (2018).
[6] A. B. Deb and N. Kjærgaard, "Radio-over-fiber using an optical antenna based on rydberg states of atoms," Appl. Phys. Lett. **112**, 211106 (2018).
[7] J. S. Otto, M. K. Hunter, N. Kjærgaard, and A. B. Deb, "Data capacity scaling of a distributed rydberg atomic receiver array," J. Appl. Phys. **129**, 154503 (2021).
[8] Y. Jiao, X. Han, J. Fan, G. Raithel, J. Zhao, and S. Jia, "Atom-based receiver for amplitude-modulated baseband signals in high-frequency radio communication," Applied Physics Express **12**, 126002 (2019).
[9] H. Li, J. Hu, J. Bai, M. Shi, Y. Jiao, J. Zhao, and S. Jia, "Rydberg atom-based am receiver with a weak continuous frequency carrier," Opt. Express **30**, 13522–13529 (2022).
[10] Z.-K. Liu, L.-H. Zhang, B. Liu, Z.-Y. Zhang, G.-C. Guo, D.-S. Ding, and B.-S. Shi, "Deep learning enhanced rydberg multifrequency microwave recognition," Nat. Commun. **13**, 1997 (2022).
[11] Z. Song, H. Liu, X. Liu, W. Zhang, H. Zou, J. Zhang, and J. Qu, "Rydberg-atom-based digital communication using a continuously tunable radio-frequency carrier," Opt. Express **27**, 8848–8857 (2019).
[12] C. L. Holloway, M. T. Simons, A. H. Haddab, C. J. Williams, and M. W. Holloway, "A "real-time" guitar recording using rydberg atoms and electromagnetically induced transparency: Quantum physics meets music," AIP Advances **9**, 065110 (2019).
[13] D. H. Meyer, K. C. Cox, F. K. Fatemi, and P. D. Kunz, "Digital communication with rydberg atoms and amplitude-modulated microwave fields," Appl. Phys. Lett. **112**, 211108 (2018).
[14] D. A. Anderson, R. E. Sapiro, and G. Raithel, "An atomic receiver for am and fm radio communication," IEEE Transactions on Antennas and Propagation **69**, 2455–2462 (2021).
[15] M. Jing, Y. Hu, J. Ma, H. Zhang, L. Zhang, L. Xiao, and S. Jia, "Atomic superheterodyne receiver based on microwave-dressed rydberg spectroscopy," Nat. Phys. **16**, 911–915 (2020).
[16] M. T. Simons, A. H. Haddab, J. A. Gordon, and C. L. Holloway, "A rydberg atom-based mixer: Measuring the phase of a radio frequency wave," Appl. Phys. Lett. **114**, 114101 (2019).
[17] V. Gerginov, F. C. S. da Silva, and D. Howe, "Prospects for magnetic field communications and location using quantum sensors," Rev. Sci. Instrum. **88**, 125005 (2017).
[18] C. Cohen-Tannoudji, J. Dupont-Roc, and G. Grynberg, "Nonperturbative calculation of transition amplitudes," in *Atom-Photon Interactions: Basic Process and Appilcations* (John Wiley & Sons, Ltd, 1998) Chap. 3, pp. 165–255.
[19] C. Holloway, M. Simons, A. H. Haddab, J. A. Gordon, D. A. Anderson, G. Raithel, and S. Voran, "A multiple-band rydberg atom-based receiver: Am/fm stereo reception," IEEE Antennas Propag. Mag. **63**, 63–76 (2021).
[20] H. Fan, S. Kumar, J. Sedlacek, H. Kübler, S. Karimkashi, and J. P. Shaffer, "Atom based RF electric field sensing," J. Phys. B **48**, 202001 (2015).
[21] C. L. Holloway, J. A. Gordon, S. Jefferts, A. Schwarzkopf, D. A. Anderson, S. A. Miller, N. Thaicharoen, and G. Raithel, "Broadband rydberg atom-based electric-field probe for si-traceable, self-calibrated measurements," IEEE Trans. Antennas Propag. **62**, 6169–6182 (2014).
[22] J. A. Gordon, M. T. Simons, A. H. Haddab, and C. L. Holloway, "Weak electric-field detection with sub-1 hz resolution at radio frequencies using a rydberg atom-based mixer," AIP Advances **9**, 045030 (2019).
[23] M. G. Bason, M. Tanasittikosol, A. Sargsyan, A. K. Mohapatra, D. Sarkisyan, R. M. Potvliege, and C. S. Adams, "Enhanced electric field sensitivity of rf-dressed rydberg dark states," New J. Phys. **12**, 065015 (2010).
[24] H. Q. Fan, S. Kumar, R. Daschner, H. Kübler, and J. P. Shaffer, "Subwavelength microwave electric-field imaging using rydberg atoms inside atomic vapor cells," Opt. Lett. **39**, 3030–3033 (2014).
[25] D. A. Anderson, S. A. Miller, G. Raithel, J. A. Gordon, M. L. Butler, and C. L. Holloway, "Optical measurements of strong microwave fields with rydberg atoms in a vapor cell," Phys. Rev. Applied **5**, 034003 (2016).
[26] M. T. Simons, J. A. Gordon, and C. L. Holloway, "Simultaneous use of cs and rb rydberg atoms for dipole moment assessment and rf electric field measurements via electromagnetically induced transparency," J. Appl. Phys. **120**, 123103 (2016).
[27] K.-Y. Liao, H.-T. Tu, S.-Z. Yang, C.-J. Chen, X.-H. Liu, J. Liang, X.-D. Zhang, H. Yan, and S.-L. Zhu, "Microwave electrometry via electromagnetically induced absorption in cold rydberg atoms," Phys. Rev. A **101**, 053432 (2020).
[28] D. H. Meyer, P. D. Kunz, and K. C. Cox, "Waveguide-coupled rydberg spectrum analyzer from 0 to 20 ghz," Phys. Rev. Applied **15**, 014053 (2021).
[29] C. L. Holloway, M. T. Simons, J. A. Gordon, and D. Novotny, "Detecting and receiving phase-modulated signals with a rydberg atom-based receiver," IEEE Antennas Wireless Propag. Lett. **18**, 1853–1857 (2019).
[30] T. F. Gallagher, *Rydberg Atoms* (Cambridge University Press, England, 1994).
[31] R. C. Brown, B. Kayim, M. A. Viray, A. R. Perry, B. C. Sawyer, and R. Wyllie, "Vhf/uhf detection using high angular momentum rydberg states," arXiv preprint arXiv:2205.12876 (2022).
[32] D. A. Anderson, E. G. Paradis, and G. Raithel, "A vapor-cell atomic sensor for radio-frequency field detection using a polarization-selective field enhancement resonator," Applied Physics Letters **113**, 073501 (2018), https://doi.org/10.1063/1.5038550.

In this experiment, we use a ladder-type four-level system to generate signals for telecommunication. The electromagnetically induced transparency (EIT) windows are generated by the control laser (480 nm) coupling the excited state ($|e\rangle$) to the Rydberg states ($|r_1\rangle$ and $|r_2\rangle$), and the microwave splits the EIT windows by Aulter-Townes (AT) effect. We set the control laser and microwave on resonance with $|e\rangle \leftrightarrow |r_1\rangle$ and $|r_1\rangle \leftrightarrow |r_2\rangle$ transitions, respectively, and the Hamiltonian reads

$$H_0 = \delta_e|e\rangle\langle e| + \delta_r\left(|r_1\rangle\langle r_1| + |r_2\rangle\langle r_2|\right) + \left(\frac{\Omega_p}{2}|e\rangle\langle g| + \frac{\Omega_c}{2}|r_1\rangle\langle e| + \frac{\Omega_{\rm LO}}{2}|r_2\rangle\langle r_1| + \text{H.c.}\right), \tag{A.1}$$

where the detunings are $\delta_e = \delta + \mathbf{k}_p\cdot\mathbf{v}$, $\delta_r = \delta + \mathbf{k}_c\cdot\mathbf{v}$. δ is the detuning of the probe laser and $\mathbf{k}\cdot\mathbf{v}$ refers to Doppler shift. $\mathbf{k}_p$, $\mathbf{k}_c$ are the wave vectors of the probe and control lasers, and $\mathbf{v}$ is the velocity of the atom that should be averaged over Maxwell-Boltzmann distribution. As for this experiment, the directions of $\mathbf{k}_p$ and $\mathbf{k}_c$ are opposite, and the distribution function of $\mathbf{v}$ is nearly a constant around the EIT windows.

The signal is applied to modulate H_0 by a Floquet Hamiltonian. As for phase-modulation (PM) and amplitude-modulation (AM), the additional term reads

$$V_F^{(\rm PM)} = \frac{\Omega_{\rm sig}}{2}\left(e^{i(\omega_{\rm sig}t+\phi_{\rm sig})}|r_2\rangle\langle r_1| + e^{-i(\omega_{\rm sig}t+\phi_{\rm sig})}|r_1\rangle\langle r_2|\right),$$
$$V_F^{(\rm AM)} = \frac{\Omega_{\rm sig}}{2}\left(|r_2\rangle\langle r_1| + |r_1\rangle\langle r_2|\right)\times \frac{1}{2}\left(1 + \sum_{n=1,3,5,\cdots}\frac{\pi}{4n}\sin n(\omega_{\rm sig}t+\phi_{\rm sig})\right). \tag{A.2}$$

Finally, considering the spontaneous decay of the excited state and Rydberg states, the effective Hamiltonian reads

$$H_{\rm eff} = H_0 + V_F - i\frac{\gamma_e}{2}|e\rangle\langle e| - i\frac{\gamma_1}{2}|r_1\rangle\langle r_1| - i\frac{\gamma_2}{2}|r_2\rangle\langle r_2|. \tag{A.3}$$

The transmission spectrum can be derived by solving the steady states of (A.3). However, as H_F is time-dependent, one needs to construct the Floquet space, where each of the four-level states is spanned with an integer, n, denoting the multiplication of the modulation frequency, such that the basis of the Floquet space is $\{|j,n\rangle | j = g,e,r_1,r_2; n = 0,\pm1,\pm2,\cdots\}$. Specifically, the matrix elements of PM Hamiltonian become

$$H_F^{(\rm PM)}{}_{mn} = \begin{cases} H_{\rm eff} - n\omega_{\rm sig} & m = n \\ \frac{\Omega_{\rm sig}}{2}e^{i\phi_{\rm sig}}|r_2\rangle\langle r_1| & m = n+1 \\ \frac{\Omega_{\rm sig}}{2}e^{-i\phi_{\rm sig}}|r_1\rangle\langle r_2| & m = n-1 \end{cases} \tag{A.4}$$

Similarly, the Floquet Hamiltonian of AM method reads

$$H_F^{(\rm AM)}{}_{mn} = \begin{cases} H_{\rm eff} - n\omega_{\rm sig} & m = n \\ \frac{\Omega_{\rm sig}}{4i}\frac{\pi}{4(m-n)}e^{i(m-n)\phi_{\rm sig}}\times \left(|r_2\rangle\langle r_1| + |r_2\rangle\langle r_1|\right) & m-n = \pm1,\pm3,\pm5,\cdots \end{cases} \tag{A.5}$$

Here we note that AM method does not include LO oscillator, but the square-wave modulation will introduce an LO term, $\Omega_{\rm LO} = \Omega_{\rm sig}/2$, to Eq. (A.1).

According to Beer-Lambert law, the transmission reads

$$T(t) = e^{-D\ \mathrm{Im}\rho_{ge}(t)}, \tag{A.6}$$

where $D = 4\pi NL|\mu_{ge}|^2/(\hbar\varepsilon_0\lambda_p\Omega_p)$ and $\rho_{ge}(t) = \sum_n \rho_{ge}^{(n)}e^{in\omega_{\rm sig}t}$. The beat signals are composed of the transitions between the cross terms in the subspaces of different frequencies, $\rho_{ge}^{(n)}$. For example, the beat signal at frequency $\omega_{\rm sig}$ reads

$$T_{\rm beat} = T_0 I_1\left(-D\sqrt{\left|\rho_{ge}^{(1)}\right|^2 + \left|\rho_{ge}^{(-1)}\right|^2 - 2\mathrm{Re}\left[\rho_{ge}^{(1)}\rho_{ge}^{(-1)}\right]}\right), \tag{A.7}$$

where T_0 is the transmission spectrum without modulation, and $I_1()$ is the modified Bessel function of the first kind. The off-diagonal elements of the density matrix, $\rho_{ge}^{(\pm1)}$ correspond to the transitions from $|g,0\rangle$ to $|e,\pm1\rangle$. The transition amplitudes can be derived with the Green's function method[18]. We truncate the Floquet space at $n = \pm1$, and consider a single atom moving with velocity v along the direction of $\mathbf{k}_p$, the matrix elements reads

$$\rho_{ge}^{(n)} = \frac{\Omega_p\Omega_s^2\Omega_{\rm LO}\Omega_{\rm sig}}{32}\left(\delta_r + \Sigma_{0,-n}^F\right)\prod_{m=0,n}\frac{1}{\delta_e^{(m)} - i\gamma/2 + \Sigma_{n,m}^R} \times \prod_{m=0,n}\frac{1}{(\delta_r^{(m)} + \Sigma_{m,1}^F)(\delta_r^{(m)} + \Sigma_{m,-1}^F) - \Omega_m^2/4}, \tag{A.8}$$

where the self energies are

$$\Sigma_{m,\pm1}^F = -\frac{\Omega_{\rm sig}^2}{2}\frac{\delta_r^{(m\pm1)}}{\delta_r^{(m\pm1)2} - \Omega_m^2/4},$$
$$\Sigma_{n,m}^R = -\frac{\Omega_c^2}{2}\frac{\delta_r^{(m)} + \Sigma_{0,-n}^F}{(\delta_r^{(m)} + \Sigma_{m,1}^F)(\delta_r^{(m)} + \Sigma_{m,-1}^F) - \Omega_m^2/4}, \tag{A.9}$$

and we denote $\delta^{(m)} = \delta - m\omega_{\rm sig}$. Apparently, the leading term of $\rho_{ge}^{(\pm1)}$ is proportional to $\Omega_{\rm LO}$ and $\Omega_{\rm sig}$ in the weak coupling limit. Additionally, $I_1(x) \approx x$ for $x \ll 1$. Therefore, it is proved that the beat signal of PM method is linearly dependent to $\Omega_{\rm sig}$. Similarly, the AM method is quadratic to $\Omega_{\rm sig}$ because $\Omega_{\rm LO}$ in Eq. (A.8) should be replaced by $\Omega_{\rm sig}/2$. Though the spectrum of the following terms are also slightly different due to the complicated Floquet interactions, the thermal average still guarantees that $\rho_{ge}^{(\pm1)} \propto \Omega_{\rm sig}^2$ for AM.

However, under relatively strong coupling condition, the high order terms will be involved. One can treat the Rydberg states numerically, then calculate the transitions from the ground state to the excited states, such that

$$\rho_{ge}^{(n)} = -\frac{\Omega_p\Omega_c^2}{8}\left(\sum_i\frac{\phi_{i,(r_1,0)}\phi_{i,(r_1,n)}^*}{E_i + i\Gamma_r/2}\right)\prod_{m=0,n}\frac{1}{\delta_e^{(n)} - i\gamma/2 + \Sigma_n^R}, \tag{A.10}$$

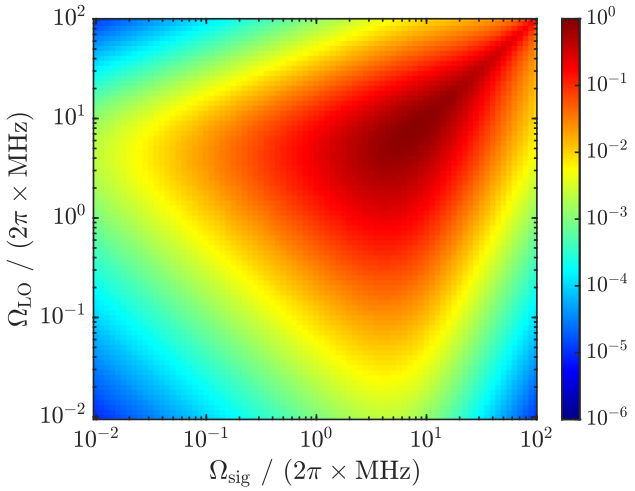

FIG. A1. Simulation of the beat signal (in arbitrary unit) of PM method for various Rabi frequency of the signal MW, Ω_{sig}, and the LO oscillator, Ω_{LO}.

where E_i and ϕ_i are eigen energies and wave functions of the tight-binding-like Hamiltonian subtracted from Eq. (A.4) or (A.5), but projected to the Rydberg subspace, $\{|r_1,0\rangle,|r_2,0\rangle,|r_1,\pm1\rangle,|r_2,\pm1\rangle,\cdots\}$, only. Γ_r refers to the decoherence of the Rydberg states, which is set to be $\sim 2\pi\times$ 6 MHz to fit the experimental results. For different Ω_{sig} and Ω_{LO}, we show the beat signal as plotted in Fig. A1. The beat signal is indeed proportional to both Ω_{sig} and Ω_{LO}, and there are optimal values for both Rabi frequencies. In experiment, the LO oscillator is optimized when $\Omega_{\mathrm{LO}} = 2\pi\times 5.63$ MHz, which agrees with the maximal values as the simulation suggests.